Quaternary Science Reviews 252 (2021) 106749

Contents lists available at ScienceDirect

Quaternary Science Reviews

journal homepage: www.elsevier.com/locate/quascirev

Abrupt climate variability since the last deglaciation based on a high-resolution peat dust deposition record from southwest China

Haijun Peng [a, b], Kunshan Bao [c, *], Lingui Yuan [d], Masao Uchida [e], Cheng Cai [f], Yongxuan Zhu [a], Bing Hong [a, b, **], Qian Guo [a, d], Hanwei Ding [a, d], Hu Yao [a, d], Yetang Hong [a]

[a] State Key Laboratory of Environmental Geochemistry, Institute of Geochemistry, Chinese Academy of Sciences, 99 Lincheng Road West, Guiyang, Guizhou, 550081, China
[b] CAS Center for Excellence in Quaternary Science and Global Change, Xi'an, 710061, China
[c] School of Geography, South China Normal University, Shipai Campus, Guangzhou, 510631, China
[d] University of Chinese Academy of Sciences, Beijing, 100049, China
[e] National Institute for Environmental Studies, Onogawa 16-2, Tsukuba, Ibaraki, 305-0053, Japan
[f] Guizhou Institute of Technology, Guiyang, Guizhou, 550003, China

ARTICLE INFO

Article history:
Received 7 July 2020
Received in revised form
24 November 2020
Accepted 4 December 2020
Available online 14 December 2020

Keywords:
Atmospheric dust
Trace elements
Rare earth elements
Last deglaciation
Asian monsoon
Peatland

ABSTRACT

The mechanism of abrupt climate changes in east Asia since the last deglaciation remains poorly explored due to the low number of high-resolution geological archives. Here we present a major and trace element including rare-earth elements (REEs) analysis of a 6 m peat archive from the Hengduan Mountains to reconstruct the rapid changes in monsoonal climate since the last deglaciation. The physicochemical parameters and Ca/Mg ratio illustrated the ombrotrophic characterization of the Yuexi peat core over the last 8800 years. Abrupt increases in dust fluxes were identified during the Old Dryas (OD), the Younger Dryas (YD), and the 4.2 kyr cold event periods. The mineral dust flux remained quite stable and low during the middle Holocene. The lowest average dust deposition rate between 8800 and 5000 cal yr BP represents a baseline of long-term atmospheric dust flux in China. The Y/ΣREE, La/Yb, Y/Yb, Y/Er indicate that deserts in northwest China, the Loess Plateau, and Tibetan soils were the dominant dust sources to the Yuexi peatland. The comparison with global climatic records suggested a teleconnection between the climate change in southwest China and North Atlantic cooling events, which implies that the abrupt variation in dust fluxes was linked with Asian monsoons variations. Our results also reveal that increased human activities significantly contribute to the dust fluxes during the late Holocene.

1. Introduction

Atmospheric mineral dust from diverse natural sources play a multifaceted role in the Earth-climate system. It affects the atmospheric material composition and radiation balance, providing nutrient input to terrestrial and marine ecosystems (Kohfeld and Harrison, 2001), but also carries chemical pollutants and various pathogens (Masson et al., 2010). In recent years, the distribution of global dust sources, the influence factors of dust input and output fluxes, and the evolution characteristics of dust storms have been intensively investigated. As an important dust source, the region of the arid eastern central Asia (AECA), east of the Pamirs Plateau, which is one of the aridest areas in the world (Yang et al., 2011), consists of widespread deserts, loess, and sandy lands. It has been considered that the summer precipitation of the AECA is under the influence of the westerlies, the Indian summer monsoon (ISM), and the East Asia Summer Monsoon (EASM) (An et al., 2012; Hong et al., 2014a; Rhodes et al., 1996; Shi et al., 2007). The long-distance transportation of dust and sands from the AECA to East Asia countries such as South Korea and Japan, and even as far as the

* Corresponding author. School of Geography, South China Normal University, Shipai Campus, Guangzhou, 510631, China.
** Corresponding author. State Key Laboratory of Environmental Geochemistry, Institute of Geochemistry, Chinese Academy of Sciences, 99 Lincheng Road West, Guiyang, Guizhou, 550081, China.
E-mail addresses: ksbao@scnu.edu.cn (K. Bao), hongbing@mail.gyig.ac.cn (B. Hong).

https://doi.org/10.1016/j.quascirev.2020.106749
0277-3791/

United States have been confirmed (Kyotani et al., 2005). Due to the influence of the complicated monsoon systems in the AECA region, the southward transportation of the AECA dust and its boundaries have been virtually unconstrained.

Peatland is an active archive for recording atmospheric environmental changes and has shown strong advantages in comprehensive identification of paleoclimate and environmental changes, which provide a very useful supplement to the global climate change database (Bao et al., 2012; Shotyk et al., 1998). Because of the high content of organic matter and plant debris, peat deposits can be precisely dated. Plants in the peatland ecosystem, such as mosses, can capture dust, thus peat archives have been widely used in the reconstruction of atmospheric dust history (e.g., Chen et al., 2020b; De Vleeschouwer et al., 2014; Le Roux et al., 2012; Li et al., 2020). In Europe and the Americas, many studies have reconstructed millennium atmospheric dust deposition history using peat records (Kylander et al., 2013, 2016; Le Roux et al., 2012; Sapkota et al., 2007). These studies are mainly carried out by means of dust flux estimation based on elemental geochemistry analysis and then reconstruct paleoclimate changes with the combination of bio-remnants such as pollen, which caused many uncertainties in tracing the dust sources. To overcome these uncertainties, radiogenic isotope signatures, such as Pb isotopes, are often used as provenance proxies as their signatures are not affected by erosion and transport (Ferrat et al., 2012a; Shotyk et al., 1998). However, Pb isotope signatures are sensitive to trace metal pollutions, which results in the source partitioning being not well constrained, especially for sites affected by anthropogenic activities (Fagel et al., 2014). Rare Earth Elements (REEs) and their isotopes (i.e., Nd and Sm), are less sensitive to trace metal pollution, and thus recent reports have gradually adopted the separation of REEs to fingerprint the dust sources (Allan et al., 2013; Fagel et al., 2014; Pratte et al., 2017).

Peatlands are widely distributed in China, specifically in northeast China and southwest China. Many studies of peat records in China are focused on temperature, precipitation, and hydrological condition reconstructions (Hong et al., 2005, 2009; Xie et al., 2013). However, there are still few reports of continuous and complete dust evolution from peat record in China. Recently, two peat geochemical studies have established the long-term history of atmospheric soil dust deposition in northern China, one shows that a decreasing dust fall trend in the past 60 years agrees well with the changes of dust storms in the past 50 years (Bao et al., 2012), the other one indicates that Holocene and late-Pleistocene aeolian mineral dust history was influenced by the long-term variations of East Asia monsoon (Pratte et al., 2020). In southwest China, the inorganic geochemistry (REEs, Sc, Y and Th) of a record form the Hongyuan peatland identified the changes in atmospheric circulation patterns and in the larger climatic arrangements of the monsoon system on the Qinghai-Tibetan Plateau during the last 9.5 ka (Ferrat et al., 2012b). However, this Holocene dust record did not capture the Younger Dryas (YD), a millennium-long cold snap, which is of particular interest to document global patterns.

Here we present a study of major and trace elements including REEs in a 15,400 years AMS ^{14}C-dated peat archive from Yuexi county, Sichuan province in southwest China. The specific objectives are 1) to reconstruct the atmospheric dust deposition history since the last deglaciation in southwest China, 2) to determine the major phases of dust deposition based on different normalized major element, trace element and REEs ratios, and 3) to interpret the atmospheric circulation patterns in terms of multi-proxies records.

2. Materials and methods

2.1. Study area

The Yuexi peatland (28°47′N, 102°57′E) is located in the west of Sichuan Province, southwest China. It is near the southeast edge of the Tibetan Plateau and northeast of Hengduan Mountains (Fig. 1), with an elevation of about 1950 m. This area has a subtropical climate controlled by the ISM. The annual average temperature is 13.1 °C. The annual average precipitation is 1130 mm, approximately 95% of which occurs in the period from May to September. The frost-free period is 247 days. The peatland covers an area of about 1 km^2 and is part of the Pear-Blossom ditch catchment which has an area about 12 km^2. The Pear-Blossom ditch runs out from the north end of the peatland and eventually flows into the Dadu River. Around the peatland, the vegetation is dominated by Yunnan pine (*Pinus yunnanensis*) and evergreen sclerophyllous oaks (*Quercus senescens*, *Quercus rehderiana*, and *Quercus gilliana*) (Hong et al., 2018).

2.2. Sample collection

In 2012, we retrieved a10-m long peat core using a Russian peat corer (Hong et al., 2018). The core was sectioned at 1 cm interval on-site and the sliced samples were stored in polyethylene bags until laboratory analysis. The plant residues in this peat core are mainly composed of vascular sedges including *Carex* and *Kobresia*, and small amounts of *Sphagnum*. The samples of the upper 30 cm section were used up for multi-parameters for previous studies (Hong et al., 2014b, 2018), and thus were not available for this study.

2.3. Physicochemical analysis

Dry bulk density (DBD, g cm^{-3}) of samples were determined by weighing a volumetric sub-sample of every 2 cm slices of the peat cores before and after drying at 55 °C for 72 h. The ash content (ASH, %) of the peat samples were estimated from the difference between the dry peat mass and the organic matter. The organic matter content was generally estimated as two times of the total organic carbon (Bao et al., 2010). The organic carbon was measured using a Vario Macro cube CHNS analyzer (vario MACRO, Elementar Analysensysteme GmbH, Germay)

2.4. Geochemical analysis

The mix-acid digestion method was used for preparing samples for geochemical analysis. Firstly, the fresh samples were dried at 55 °C for 72 h and then grounded. For sample digestion, 100 mg of grounded sample was put into a Teflon tube, with 0.2 ml 48% HF and 2 ml 68% HNO_3, and then the Teflon tubes were heated in the oven at 150 °C for 24–30 h. After heating, the tubes were put at room temperature for cooling down, then the digested samples were evaporated on an electric heating board till the samples crystallized, and then 1 ml 68% HNO_3 was added with continued heating. After the water in the sample evaporated completely, 1 ml Rh internal standard, 2 ml 68% HNO_3, and 3 ml milli-Q water were added. Then the samples were sealed and put into an oven at 140 °C for 4–5 h. The samples were reserved at a constant volume of 100 ml. Major elements (K, Ca, Mg, Fe) were measured by ICP-OES (Leeman Prodigy, USA), and trace elements (Cu, Hf, Pb, Rb, Sr, Y, Zr) and REEs were measured by ICP-MS (ELAN DRC-e, PerkinEmer,

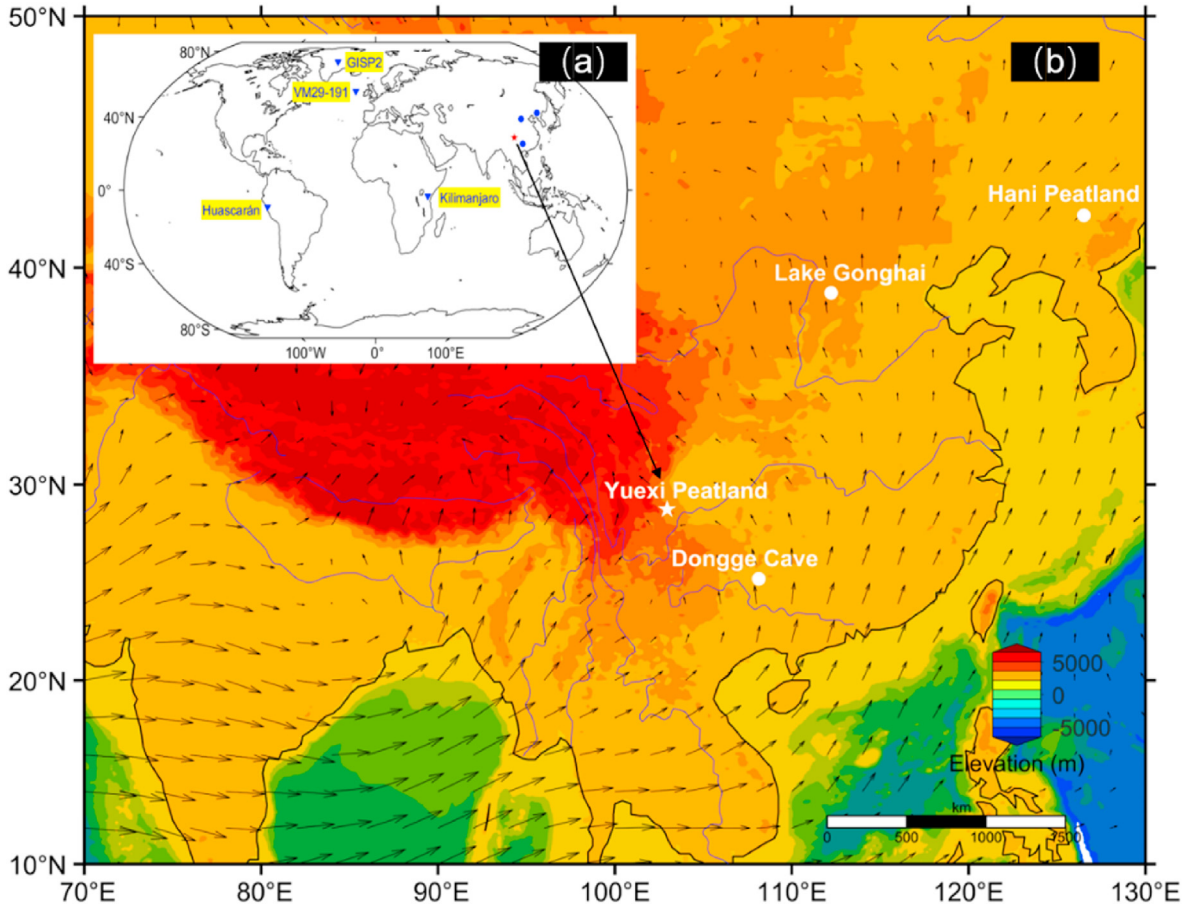

Fig. 1. Location of the study area and other reference sites: (a) the GISP2 ice core (Stuiver et al., 1995), the Kilimanjaro ice core (Thompson et al., 2002), the ocean sediment record from VM 29–191 (Bond et al., 2001), the Dongge Cave stalagmite (Dykoski et al., 2005), the Gonghai lake sediment (Chen et al., 2020a), the Hani peatland (Pratte et al., 2020), and the Yuexi peatland (this study). (b) Location of study site and averaged wind field at 850 hPa in summer (from June to August) from 1851 to 2014 (wind field data retrieved from the NOAA-CIRES 20th Century Reanalysis V2c) (Compo et al., 2006).Terrain data retrieved from the NOAA Data Announcement 88-MGG-02 (https://www.ngdc.noaa.gov/mgg/global/etopo5.HTML) on7 March 2019.

USA) at the State Key Laboratory of Environmental Geochemistry, Institute of Geochemistry, Chinese Academy of Sciences.

Several reference standards, AGV (USGS AGV-2 andesite), AMH (USGS AMH-1 Mount Hood andesite), and GBPG (USGS GBPG-1 garn-biot-plag-gneiss) were used for quality control of the metal analysis. Samples of the reference material were analyzed along with each batch of peat samples to provide a check on the analysis of the peat material. Average measured concentrations of trace metals for these reference materials, and their respective certified values as well as the blank values are given in Table 1. The precision of the measurements was tested on replicate analyses of some randomly selected samples and the results of trace metals concentrations were also summarized in Table 1.

2.5. Age-depth model

Age models for the whole core were constructed from 29 radiocarbon AMS dates (AMS ^{14}C) of peat cellulose samples that were measured at the AMS Laboratory of the National Institute for Environmental Studies in Tsukuba, Japan. The obtained age of the base was 33,300 cal year BP after the CALIB-4.3 calibration (Hong et al., 2018). In this study, an updated age model was developed based on 20 AMS ^{14}C dates for the upper 6 m of the peat core (Hong et al., 2014b), using the Bayesian model (Bacon 2.2) in R language (Blaauw and Christen, 2011). This Bayesian model (Fig. 2) is significantly correlated with the previous linear interpolation model ($r = 0.999$, $P < 0.001$) (Hong et al., 2014b). The upper 5.6 m section of the peat core represents a sequence 15,400 cal yr BP in length which documents the climatic change history since the last deglaciation, with a mean accumulation rate of 0.5 mm yr^{-1}. The peat core section from 30 cm to 566 cm was used for reconstructing the atmospheric dust deposition, and a total of 269 slice-samples were analyzed for major and trace element content. The mean resolution of our reconstruction is around 55 years.

2.6. Data calculation and analysis

The dust accumulation rate is calculated from a conservative lithogenic element concentration, dry bulk density and the sedimentation rate using the procedure outlined by (Shotyk et al., 2002).

$$\mathrm{AR\,dust} = \left([\mathrm{Element}]_{\mathrm{sample}} \Big/ [\mathrm{Element}]_{\mathrm{UCC}}\right) \times \mathrm{DBD} \times \mathrm{SR} \times 10000$$

where AR dust is dust flux (g m^{-2} yr^{-1}), the [Element]$_{\mathrm{sample}}$ and [Element]$_{\mathrm{UCC}}$ are the lithogenic elements concentrations in a sample and in the Earth's upper continental crust (UCC) (Wedepohl, 1995), DBD is the sample's dry bulk density (g cm^{-3}) and SR is the sedimentation rate (cm yr^{-1}). The estimation of net dust flux depends on the lithogenic elements used to calculate it

Table 1
Recovery and reproductivity from Certified Reference materials (CRMs), including AGV (USGS AGV-2 andesite), AMH (USGS AMH-1 Mount Hood andesite), GBPG (USGS GBPG-1 garn-biot-plag-gneiss). These CRMs certified values and the blank values are also shown. Replicate analyses of the trace metals are with respect to some randomly selected samples. All values are means and standard deviations; mg kg^{-1}.

Material	Cu65	Pb206	Rb85	Sr86	Hf179	Y89	Zr91	La139	Ce140	Pr141	Nd146	Sm147	Eu151	Gd157	Tb159	Dy163	Ho165	Er166	Tm169	Yb174	Lu175
Blank (n = 8)	0.01	−0.01	0.08	0.02	0.00	0.01	0.07	0.01	0.01	0.00	−0.02	−0.01	0.00	0.00	0.00	0.00	0.00	0.00	0.00	0.00	0.00
	0.19	0.08	0.04	0.21	0.00	0.01	0.09	0.01	0.03	0.00	0.02	0.04	0.00	0.01	0.00	0.00	0.00	0.00	0.00	0.00	0.00
AGV (n = 15)	52.43	14.26	67.49	664.13	5.12	19.15	231.13	39.27	70.53	8.19	30.37	5.40	1.53	4.56	0.69	3.40	0.69	1.85	0.27	1.62	0.26
	4.00	0.64	1.01	13.28	0.27	0.45	4.78	0.94	1.69	0.19	1.05	0.20	0.05	0.19	0.02	0.11	0.03	0.10	0.02	0.09	0.02
GBW (n = 3)	5.96	48.13	4.29	235.67	0.24	0.84	8.82	1.22	2.48	0.26	0.94	0.19	0.03	0.15	0.03	0.13	0.03	0.08	0.01	0.06	0.01
	0.41	0.84	0.06	1.53	0.16	0.04	5.63	0.11	0.15	0.02	0.07	0.02	0.01	0.02	0.00	0.02	0.00	0.02	0.00	0.01	0.00
AMH (n = 15)	33.38	10.27	19.65	572.13	3.65	15.45	147.87	17.59	37.04	4.38	17.41	3.52	1.17	3.31	0.53	2.84	0.56	1.54	0.21	1.32	0.20
	1.72	0.35	0.49	12.57	0.20	0.44	3.72	0.49	0.91	0.14	0.67	0.20	0.04	0.13	0.02	0.17	0.03	0.07	0.01	0.06	0.02
GBPG (n = 18)	32.31	13.66	57.14	388.39	5.03	18.37	202.39	52.64	100.62	11.91	42.87	6.61	1.79	4.74	0.66	3.15	0.68	2.07	0.31	2.03	0.31
	2.25	0.61	1.65	10.78	0.34	0.47	6.69	1.41	2.83	0.32	1.76	0.31	0.06	0.24	0.02	0.13	0.03	0.09	0.01	0.10	0.01
Peat (48 cm)	7.68	14.47	35.33	33.47	0.97	11.07	39.97	16.37	32.07	3.55	13.00	2.43	0.48	2.09	0.34	1.80	0.37	1.04	0.14	0.95	0.13
	0.17	0.51	0.78	0.95	0.08	0.06	0.80	0.58	1.54	0.12	0.52	0.14	0.01	0.09	0.02	0.03	0.02	0.06	0.02	0.08	0.00
Peat (58 cm)	10.75	10.90	16.70	25.45	0.50	9.39	17.70	9.86	21.65	2.37	9.66	1.93	0.44	1.88	0.29	1.60	0.31	0.93	0.12	0.77	0.11
	1.33	0.71	0.85	0.92	0.03	0.33	0.57	0.35	1.20	0.20	0.47	0.11	0.02	0.00	0.03	0.08	0.01	0.04	0.00	0.04	0.01
Peat(108 cm)	4.00	5.10	2.42	17.55	0.08	4.42	3.97	3.48	8.61	0.97	3.97	0.96	0.20	0.89	0.14	0.75	0.15	0.41	0.06	0.33	0.05
	0.69	0.23	0.02	0.21	0.01	0.08	0.18	0.10	0.08	0.02	0.03	0.02	0.02	0.01	0.00	0.01	0.01	0.00	0.00	0.01	0.01
Peat (138 cm)	7.68	8.84	33.30	17.40	0.85	7.10	31.85	8.92	17.70	2.08	7.80	1.52	0.32	1.41	0.23	1.23	0.25	0.74	0.11	0.65	0.10
	0.32	0.06	0.14	0.28	0.09	0.05	0.78	0.13	0.00	0.04	0.01	0.06	0.03	0.06	0.00	0.01	0.00	0.01	0.01	0.01	0.00
Peat (160 cm)	7.83	7.68	14.30	14.40	0.34	5.18	12.25	5.18	11.55	1.35	5.35	1.09	0.25	1.10	0.17	0.89	0.17	0.49	0.07	0.43	0.07
	0.57	0.39	0.28	0.42	0.07	0.08	0.07	0.13	0.21	0.01	0.06	0.03	0.00	0.02	0.01	0.03	0.01	0.01	0.01	0.03	0.01
Peat (214 cm)	11.88	9.80	16.35	17.20	0.48	7.48	18.20	7.44	16.70	1.85	7.26	1.60	0.34	1.52	0.24	1.40	0.26	0.75	0.10	0.60	0.09
	0.37	0.01	0.07	0.28	0.04	0.08	0.28	0.33	0.42	0.11	0.36	0.00	0.00	0.01	0.00	0.05	0.00	0.01	0.01	0.02	0.00
Peat (260 cm)	9.86	5.84	12.15	16.95	0.29	4.36	10.70	4.90	11.20	1.13	4.60	0.80	0.19	0.91	0.14	0.76	0.15	0.44	0.06	0.37	0.06
	1.84	0.09	0.21	0.49	0.03	0.12	0.00	0.23	0.71	0.05	0.07	0.08	0.04	0.06	0.01	0.01	0.00	0.00	0.00	0.01	0.00
Peat (296 cm)	8.63	6.79	41.60	21.25	1.04	6.22	38.35	8.99	16.95	2.00	7.31	1.35	0.27	1.17	0.18	1.01	0.22	0.66	0.10	0.63	0.10
	1.04	0.11	0.57	0.35	0.01	0.03	1.06	0.11	0.21	0.04	0.07	0.04	0.02	0.03	0.02	0.04	0.01	0.04	0.01	0.03	0.01
Peat (328 cm)	11.20	11.15	26.00	21.45	0.80	7.39	31.80	9.89	21.20	2.17	8.27	1.59	0.35	1.49	0.22	1.22	0.26	0.78	0.11	0.68	0.10
	0.42	0.07	0.14	0.21	0.03	0.12	0.14	0.04	0.28	0.03	0.06	0.03	0.02	0.06	0.01	0.00	0.02	0.03	0.00	0.05	0.00
Peat (364 cm)	7.13	3.87	8.51	15.75	0.24	3.32	9.73	3.64	7.86	0.84	3.39	0.70	0.16	0.60	0.10	0.54	0.11	0.34	0.05	0.27	0.04
	1.91	0.33	0.10	0.07	0.00	0.05	0.81	0.03	0.08	0.00	0.09	0.03	0.00	0.01	0.00	0.03	0.00	0.03	0.00	0.02	0.00
Peat (396 cm)	12.00	8.78	21.35	22.75	0.74	7.39	32.05	10.07	20.95	2.24	8.07	1.54	0.32	1.52	0.23	1.28	0.26	0.69	0.10	0.61	0.09
	0.28	0.09	0.64	0.92	0.01	0.16	0.35	0.19	0.92	0.09	0.51	0.03	0.03	0.04	0.01	0.01	0.01	0.00	0.00	0.01	0.00
Peat (418 cm)	10.85	11.95	24.50	27.60	1.29	9.97	51.45	13.75	28.45	3.05	11.45	2.15	0.45	2.09	0.33	1.70	0.35	0.99	0.14	0.90	0.14
	0.07	0.21	0.85	1.41	0.03	0.47	0.49	0.35	0.64	0.01	0.07	0.09	0.05	0.13	0.00	0.07	0.01	0.03	0.00	0.01	0.00
Peat (436 cm)	13.75	18.75	39.55	31.70	1.82	13.80	68.70	19.75	38.75	4.42	15.75	2.89	0.64	2.79	0.45	2.30	0.49	1.36	0.19	1.26	0.19
	0.64	0.07	0.49	0.28	0.01	0.14	0.57	0.07	0.35	0.07	0.07	0.09	0.02	0.10	0.01	0.00	0.01	0.03	0.01	0.06	0.00
Peat (476 cm)	16.20	19.80	24.45	21.15	1.17	9.12	43.10	12.90	26.45	2.81	10.70	2.06	0.40	1.72	0.29	1.65	0.32	0.92	0.13	0.81	0.12
	0.28	0.28	0.35	0.07	0.04	0.04	0.28	0.14	0.49	0.03	0.42	0.15	0.02	0.02	0.00	0.01	0.00	0.02	0.01	0.04	0.01
Peat (502 cm)	19.25	17.25	25.95	29.90	1.57	13.05	61.85	16.95	34.95	3.82	13.55	2.71	0.59	2.53	0.43	2.27	0.45	1.30	0.18	1.10	0.17
	0.07	0.35	0.21	0.14	0.01	0.07	1.63	0.35	0.64	0.05	0.07	0.01	0.03	0.07	0.00	0.09	0.02	0.04	0.01	0.04	0.00
Peat (538 cm)	21.80	17.55	42.10	25.05	1.51	10.01	57.95	14.95	29.20	3.36	12.10	2.22	0.45	1.95	0.33	1.72	0.36	1.01	0.15	0.98	0.16
	0.71	0.07	0.71	0.35	0.10	0.13	0.49	0.07	0.14	0.04	0.14	0.00	0.00	0.04	0.01	0.02	0.00	0.03	0.01	0.01	0.00
Peat (558 cm)	23.55	15.95	39.70	37.55	2.09	14.40	79.35	19.45	38.60	4.38	16.60	3.10	0.64	2.68	0.45	2.51	0.50	1.48	0.21	1.32	0.19
	0.07	0.35	1.13	0.21	0.01	0.28	1.20	0.21	0.14	0.03	0.14	0.04	0.01	0.07	0.01	0.04	0.01	0.03	0.00	0.06	0.01

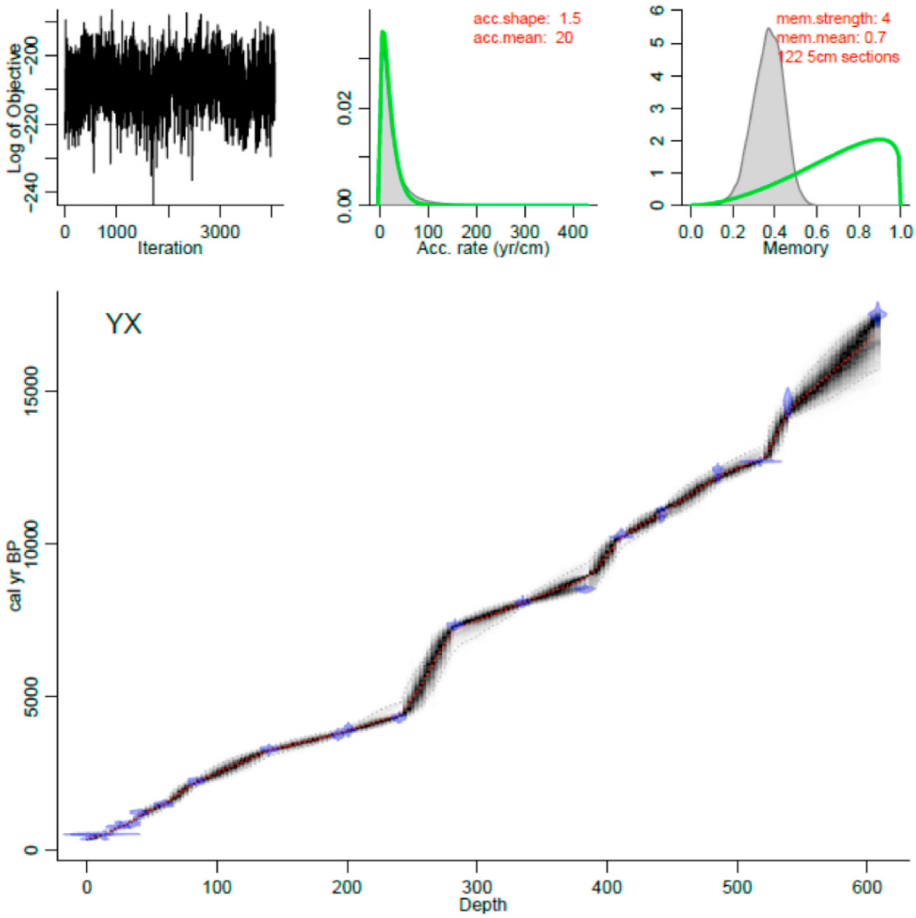

Fig. 2. Simulated relationship between calibrated yrs BP (1950 CE) and depth by Bacon Model using AMS ^{14}C age data for the Yuexi peat core. Grayscale represents age model probability and is bounded by a dotted-line confidence interval (95%); the darkest grey color indicates the highest probability age for that depth. The red line shows the weighted average age data used in this paper. (For interpretation of the references to color in this figure legend, the reader is referred to the Web version of this article.)

(Allan et al., 2013; Cortizas et al., 2020; Kylander et al., 2016), and thus here the Zr and the sum of REEs (ΣREE) were used to calculate the natural and total dust fluxes, respectively; their difference was regarded as the anthropogenic dust flux.

Enrichment factor (EF) relative to UCC is used to characterize the concentrations and sources of trace metals (Bao et al., 2012; Shotyk et al., 2002), the equation is described as below.

$$EF = (TE/Zr)_{sample} \Big/ (TE/Zr)_{UCC}$$

where TE is the trace element (Cu, Pb and REEs), and the reference element takes Zr due to its significant correlations given in the results.

Descriptive statistical analyses were conducted to calculate the means, ranges, and standard deviations of the peat parameters. Pearson correlation coefficients were calculated to evaluate the relationships among the individual parameters. These procedures were performed using the SPSS 11.5 software package (SPSS, 2002). Statistical significance was determined at the P = 0.05 level except if indicated differently.

3. Results

3.1. Physicochemical properties of peat

The average ASH of the Yuexi peat core is 14.4%. The ASH fluctuated while showing a major peak at 480 cm depth (12,180 cal yr BP). Following this peak, the ASH decreased and stabilized at a low level from 380 cm to 272 cm (8800–6500 cal yr BP), with an average of 4.7%. After this steady state, the ASH increased gradually and reached a peak at 178 cm (3760 cal yr BP). Finally, the ASH fluctuated with an increasing trend with depth (Fig. 3). The TOC profile mirrored the ASH. The TOC ranged from 16 to 50% for the whole core, with an average of 42.8%. The DBD of the peat core ranged from 0.05 to 0.37 g cm^{-3}, with an average of 0.13 g cm^{-3} for the whole core. The depth variation of DBD was significantly correlated with that of the ASH ($r = 0.702$, $P < 0.001$). For the steady period (8800–6500 cal yr BP), the average DBD and TOC were 0.10 g cm^{-3} and 47.6%, respectively.

3.2. Major and trace elements

Profiles of major elements (Ca, Mg, Fe) and trace elements (Cu, Hf, Pb, Rb, Sr, Y, Zr) contents are presented in Fig. 4. The variations in Ca, Mg and Fe content are different. The Ca increased with depth below ca. 272 cm (6500 cal yr BP), with an abnormal value at 530 cm depth; then it decreased to 178 cm depth (3760 cal yr BP); finally, it increased with depth. The variation of Mg was small along the whole profile, but presented two peaks at 480 cm depth (12,180 cal yr BP) and 178 cm depth (3760 cal yr BP). The variations in Fe contents were characterized by a relatively constant state below 272 cm (6500 cal yr BP), with a major peak at 480 cm depth (12,180 cal yr BP) like the variation patterns of Mg, and an obvious

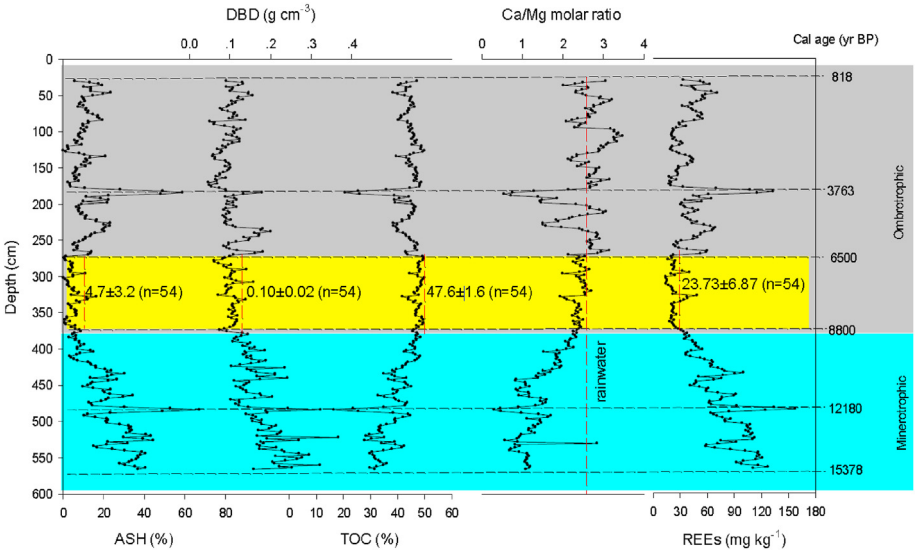

Fig. 3. Depth profiles of the ash content (ASH, %), total organic carbon (TOC, %), the dry bulk density (DBD, g cm-3), the molar ratio of Ca/Mg, and the summary of rare earth elements (REEs, mg kg^{-1}) of the Yuexi peat core. The averages of ASH, TOC, DBD and REEs in the stable section identified by the change point analysis (corresponding to 8800-6500 cal yr BP) are regarded as baseline in China. The boundary between ombrotrophic and minerotrophic sections is also indicated.

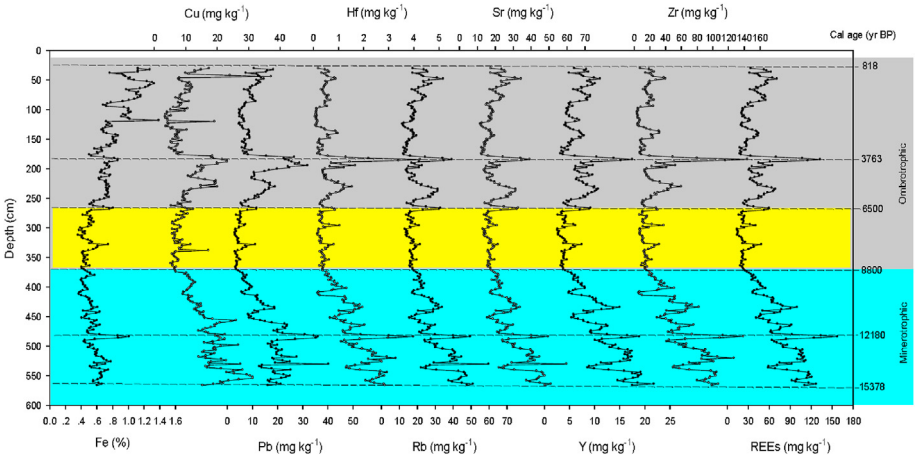

Fig. 4. Yuexi core peat: depth profiles of the major and trace elements and REEs also included for comparison. The yellow section corresponds to the stable period of the ASH changing point analysis. (For interpretation of the references to color in this figure legend, the reader is referred to the Web version of this article.)

Table 2
Pearson correlation coefficients (r) between the trace elements and the sum of REEs ($n = 269$).

	Cu	Rb	Sr	Y	Zr	Hf	Pb	∑REE
Cu	1							
Rb	.689**	1						
Sr	.665**	.730**	1					
Y	.736**	.767**	.939**	1				
Zr	.740**	.865**	.898**	.931**	1			
Hf	.735**	.879**	.891**	.924**	.996**	1		
Pb	.773**	.798**	.732**	.811**	.795**	.801**	1	
∑REE	.745**	.842**	.933**	.980**	.959**	.954**	.837**	1

**. Correlation significant at the 0.01 level (2-tailed).

increase with depth upward above 272 cm.

The analyzed 7 trace elements are significantly correlated with each other ($r > 0.41$, $P < 0.001$; Table 2). Their depth distributions are consistent and similar to REEs (Fig. 4). They fluctuated below 480 cm depth and formed a major peak at 480 cm depth (12,180 cal yr BP). Then, they decreased with depth upward, and became relatively constant from 380 cm to 272 cm (8800–6500 cal yr BP). After that, they gradually increased and reached a peak at 178 cm depth (3760 cal yr BP). Finally, they increased with depth with some small fluctuations (Fig. 4).

3.3. REEs content of the core

Except for Pm which does not occur naturally in the Earth's crust, the other 14 REEs are relatively abundant in the rocks and soils, and thus were measured in this paper. Overall concentration ranges for each REEs and their sum were summarized in Table 3. All REEs are significantly correlated with each other ($r > 0.95$, $P < 0.001$). The correlation coefficients indicate that individual REEs vary in the same manner with their sum and the ASH content (Fig. 5). A fluctuating pattern was observed below 480 cm. A decreasing trend was observed from 480 cm to 380 cm. Then the

Table 3
The mean, maximum and minimum concentrations of 14 REEs (mg kg^{-1}) in peat core taken from Yuexi peatland, southwest China ($n = 269$).

	La	Ce	Pr	Nd	Sm	Eu	Gd	Tb	Dy	Ho	Er	Tm	Yb	Lu	∑REE
Minimum	2.61	5.84	0.63	2.54	0.50	0.11	0.47	0.07	0.40	0.08	0.24	0.03	0.21	0.03	13.99
Maximum	37.00	63.80	8.28	29.60	4.99	0.92	3.88	0.70	3.89	0.79	2.30	0.33	2.19	0.33	157.63
Mean	10.49	21.41	2.40	8.97	1.72	0.36	1.57	0.25	1.38	0.28	0.81	0.11	0.73	0.11	50.59
Std. Dev.	6.67	12.31	1.47	5.22	0.94	0.19	0.77	0.13	0.74	0.15	0.44	0.06	0.42	0.06	29.46

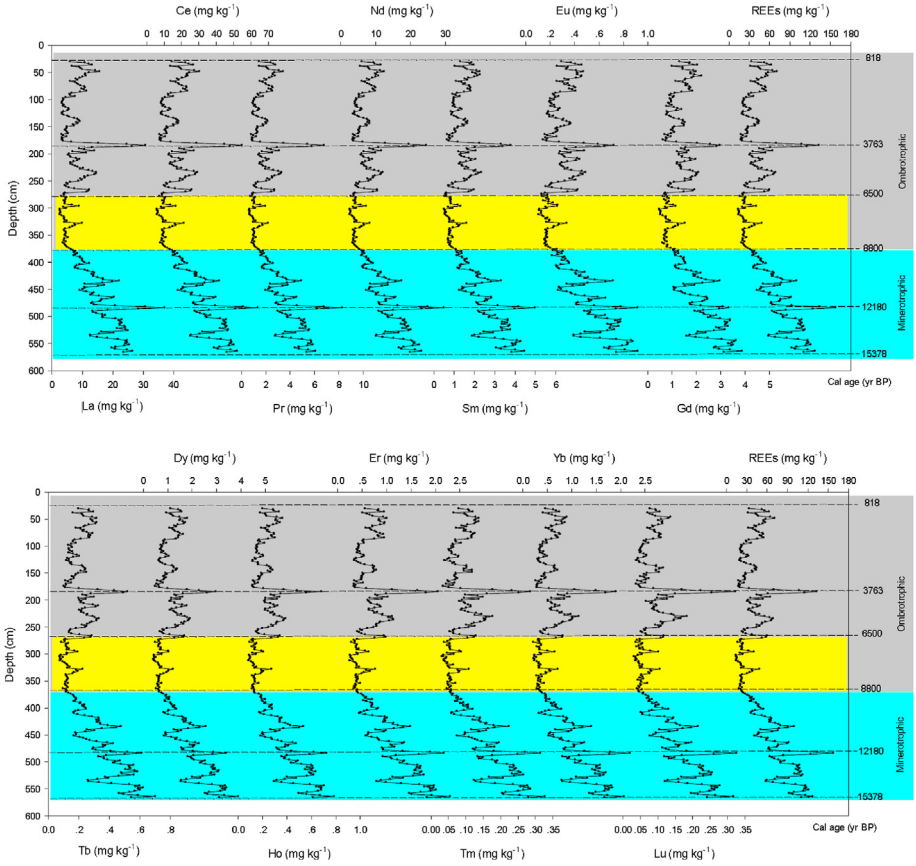

Fig. 5. Yuexi core peat: depth profiles of the 14 rare earth elements and their sum (REEs). The yellow section corresponds to the stable period of the ASH changing point analysis. (For interpretation of the references to color in this figure legend, the reader is referred to the Web version of this article.)

REEs were relatively constant, with an average of 23.73 ± 6.87 mg kg^{-1} (Fig. 3). An increasing trend was observed from 272 cm to 178 cm, at which point, a peak occurred. Above 178 cm, the REEs fluctuated with a minor increase upward.

3.4. Atmospheric dust deposition rate

The ombrotrophic peat section records an 8800-year history of atmospheric dust deposition in the Yuexi peatland (Fig. 6). The profiles of atmospheric dust deposition rate calculated using Zr and ΣREE were very similar, which is due to the positive correlation between Zr and REEs concentrations ($r = 0.97$, $P < 0.001$, $n = 269$). The dust flux based on Zr represents the history of natural atmospheric dust deposition in the Yuexi peatland. The relatively lower natural dust deposition rate is 3.8 g m^{-2} yr^{-1} observed between 8800 and 5000 cal yr BP (the middle Holocene), which could represent a baseline in southwest China.

4. Discussion

4.1. Peat trophic status

Ombrotrophic peatlands are exclusively fed by atmospheric inputs and are characterized by low water table fluctuation, low pH (<5), low bulk density (0.05–0.1 g cm^{-3}), and low ash content (<10%). By contrast, minerotrophic peatlands receive inputs from atmosphere deposition and from surrounding rocks weathering and soils erosion, with important water table fluctuation, a higher pH (up to 8), and relatively higher signatures in density and ash content (Sapkota et al., 2007; Shotyk, 1996). The pH of the surface peat reported as 5.5–6.5 (Li et al., 2016a). The average ASH and DBD in the peat sections between 272 and 380 cm (8800–6500 cal yr BP) and above 178 cm (the last 3760 cal yr BP) are lower than the maximum limit of ombrotrophic signature. For most of the peat section upper 380 cm, TOC is higher than the TOC 30% of typical ombrotrophic peat.

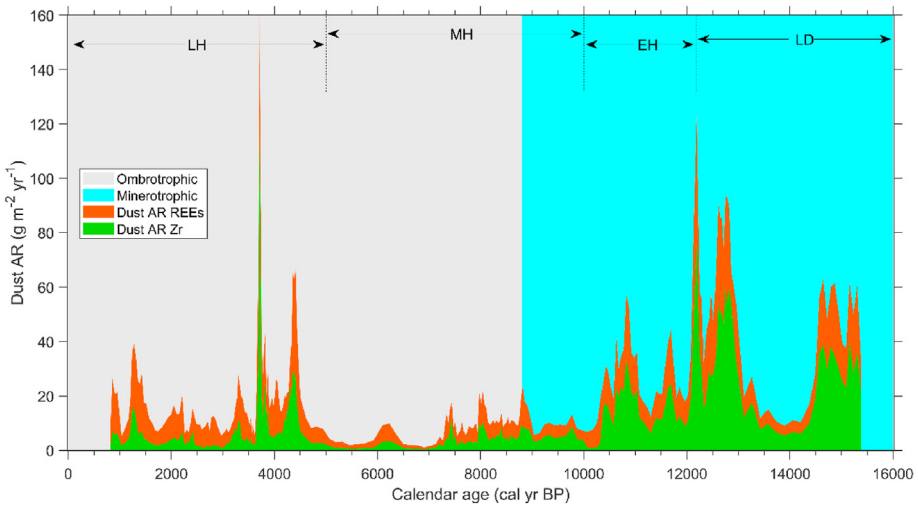

Fig. 6. Yuexi core peat: temporal variations of atmospheric dust flux (Dust AR, g m^{-2} yr^{-1}) reconstructed from the REEs-based (total) and Zr-based (natural) Dust AR. The boundary between ombrotrophic and minerotrophic peat is also indicated.

In addition, the Ca/Mg ratio had been widely applied in geochemical evaluation on the ombrotrophic and minerotrophic peat boundary (Pratte et al., 2020; Shotyk, 1996; Steinmann and Shotyk, 1997). The molar ratio of Ca/Mg in the upper 380 cm of the Yuexi peat core is similar to the value of regional rainwater (2.7) at a semi-rural site in Ya'an (150 km north of Yuexi county), Sichuan basin (Li et al., 2016b). According to those parameters, the Yuexi peat core can be divided into two section: ombrotrophic peat above 380 cm (the last 8800 cal yr BP) and minerotrophic peat below 380 cm. The ombrotrophic peat sections were used for estimating atmospheric dust deposition.

4.2. Preliminary dust province

The Yuexi peatland is at the southeast edge of the Tibetan Plateau, and the soil mineral from the Tibetan Plateau would be the local source to the mineral composition in the peat. Being located at the margins of the East Asian and Indian monsoon systems, the Yuexi peatland is probably affected by the long-distance transport of desert dust from both the AECA and India (Shao et al., 2011). Trace elements and REEs ratios can be used for dust provenance-tracing. A detailed geochemical assessment of the Hongyuan peat in the same region with the Yuexi peatland suggested that the provenance tracers (Y/ΣREE, La/Yb, Y/Yb, Y/Er, etc.) were particle-size-independent tracers and could be used to the long-range provenance tracing of Asian dust with respect to the bulk sample analysis (Ferrat et al., 2011). Therefore, in this study, the Y/ΣREE, La/Yb, Y/Yb, Y/Er proxies were used to perform a preliminary source assessment to distinguish the Indian Thar desert, the Chinese deserts, the Chinese Loess plateau and the Tibetan soils. The Eu anomaly (Eu/Eu*) was not used because it was probably affected by the particle size to some extent (Ferrat et al., 2011). The ratios of La/Yb, Y/ΣREE and Y/Yb were normalized to the Post Archean Australian Shale (PAAS) (McLennan, 1985).

The bivariate plots show that the Yuexi peat samples overlap with the domains of the Chinese deserts and/or Chinese Loess plateau as well as the Tibetan local soils; however, are clearly separated from the Indian Thar desert domain (Fig. 7A, B, C). This suggests that the Indian Thar desert did not contribute mineral matter to the Yuexi peatland during the last deglaciation and the Holocene. The reason that dust from the Thar desert did not reach the Hengduan Mountains could be attributed to the in-phase moisture content and monsoon intensity pattern of the ISM. Since desert dust aerosol levels can rapidly modulate monsoon rainfall over central India, most of the northward transportation of the Thar dust has been deposited in the south of the Qinghai-Tibetan Plateau (Vinoj et al., 2014). As for the southward transportation of dust from the Loess Plateau and deserts in northwest China, it has been suggested that colder ACEA could increase dust storm intensities and hence promote the long-distance aeolian penetration into northeast China and southwest China (Chen et al., 2020a; Zhang et al., 2020a, 2020b).

In addition, peat averages of $(La/Gd)_N$ and $(Gd/Yb)_N$ were 0.78 and 1.34, and thus, the REEs patterns of the Yuexi peat samples from all phases were relatively flat, with values a little higher for middle REEs (Sm - Tb) than for the light REEs (La - Nd) and the heavy REEs (Dy - Lu) (Fig. 7D). The average $(Eu/Eu^*)_N$ was 1.04 ± 0.06, which suggested the Europium anomaly was absent in the Yuexi record. There were very similar characteristics of the REEs patterns in the Yuexi record during the different events periods with those of the potential dust sources in China (the Chinese deserts, Chinese Loess plateau and the Tibetan local soils). However, the difference of REEs between the Yuexi peat and the Indian Thar desert can be still observed (Fig. 7D). This was probably because the Thar desert had flatter light REE, more negative heavy REE fraction and Europium anomalies (Ferrat et al., 2011). Thus, our results that combined the REEs patterns with the normalized source tracing proxies, confirmed the previous conclusion that the Indian Thar desert dust could not input into the Tibetan Plateau during the last deglaciation and Holocene, due to the Himalayan mountain range as a physical barrier for dust transportation (Ferrat et al., 2012b).

Due to the slight variations in REEs pattern among the different phases, the contributions from different potential dust sources would be constant over the last deglaciation and Holocene. We applied the average REEs and Y contents of the whole Yuexi peat core in the source end-members mixing model (Li et al., 2020) to estimate the contribution of the local (Tibetan Plateau soil) and distal sources (Chinese deserts and Loess) to the Yuexi peatland. The calculations showed that the contributions of the Chinese deserts, Loess Plateau and Tibetan Plateau were 45%, 22% and 33%, respectively. It is worth noting that the Loess Plateau is also an important dust source to southwest China.

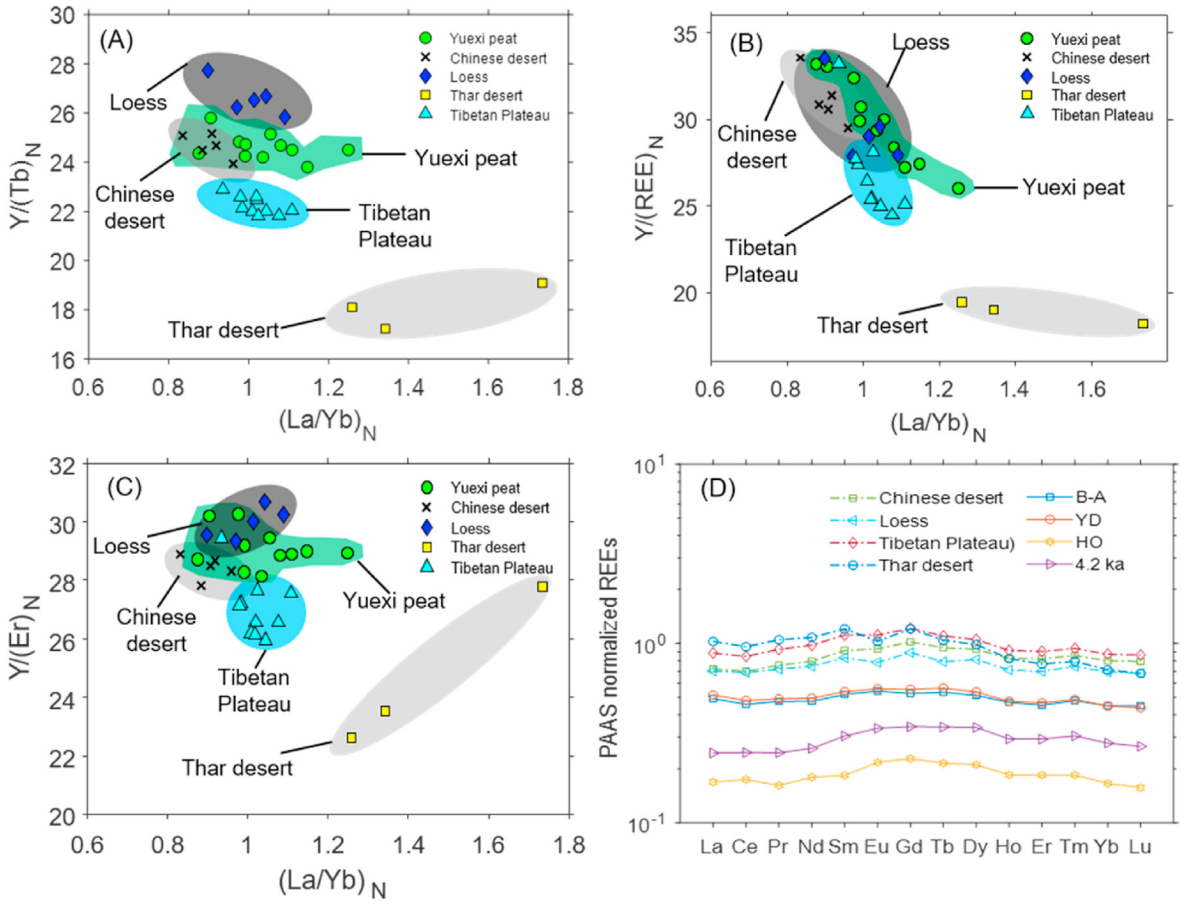

Fig. 7. Bivariate plots of Y/Tb_N versus $(La/Yb)_N$ (A), $Y/(REE)_N$ versus $(La/Yb)_N$ (B) and Y/Er_N versus $(La/Yb)_N$ (C), and the REEs patterns (D). The ratios of $(La/Yb)_N$, Y/Tb_N, $Y/\Sigma REE_N$ and Y/Er_N were averaged for 4 periods showing the composition of the Yuexi peat samples: during the 4.2 kyr cold event, during the HO period, during the YD, and B-A periods. Data on the Chinese deserts (Qaidam basin and Taklamakan, Tengger and Badain Jaran deserts, n = 5), the Chinese loess plateau (n = 5), the Thar desert (n = 3) and the eastern Tibetan soils (n = 9) were obtained from elsewhere (Ferrat et al., 2011). The N subscript indicates that values are normalized to PAAS (McLennan, 1985).

4.3. Dust deposition history

The calculated natural dust flux sequence was compared with global climatic change proxies (Fig. 8). Higher natural dust flux in Yuexi peat in 15,400–14,700 cal yr BP (the Oldest Dryas (OD)) and lower dust flux in 14,700–12,900 cal yr BP (the Bølling-Allerød (B-A) warm periods) were observed. The Yuexi peat record began with a major peak of dust flux in the period of 12,900–11,700 cal yr BP, which indicates that the climate of the southwest China region during the Younger Dryas (YD) was cold and dry. These were consistent with the $\delta^{18}O$ records of the GISP2 Greenland ice core (Stuiver et al., 1995) and the Dongge Cave stalagmite (Dykoski et al., 2005).

During the YD, increased dust deposition had been also reported by peat records in Switzerland (Le Roux et al., 2012), Tierra del Fuego (Vanneste et al., 2016), and Northeast China (Pratte et al., 2020). Therefore, the consistency of YD dust records in peat archives show an increased atmospheric dust load and cold-dry climate over the world during the YD stadial. In the middle Holocene (10,000–5000 cal yr BP), the dust deposition flux was quite stable and low, which is an indicator of the warm phase as the Holocene Megathermal. In particular, the lowest dust deposition occurred between 7000 and 5000 cal yr BP, indicating the most warm and humid climate period which was named as the Holocene Optimum (HO) (Renssen et al., 2009). This HO period corresponds well with the peak warmth as reflected by the pollen and geochemical records of lakes across East Asia (Gao et al., 2019; Jiang et al., 2019). In the early Holocene, a major dust peak occurred in 3900–4500 cal yr BP, which is coincident with the "4.2 kyr" cold and dry event. This major dust peak in the Yuexi peat record also agreed well with the dust event recorded in ice cores from Huascarán in the Andes of Northern Peru (Thompson et al., 2000) and from Kilimanjaro in tropical Africa (Thompson et al., 2002), this may suggest a widespread drought happened in the mid-low latitude area during this period, which had a huge impact on the decline of civilizations (Cullen et al., 2000).

4.4. The dynamic mechanism for dust deposition

The Yuexi dust deposition history displayed a similar pattern of climate change as the world-wide geological records (Fig. 8), suggesting a precise teleconnection between southwest China and the North Atlantic cooling during the last deglaciation and Holocene. It had been reported that the sea ice and thermocline circulation in the North Atlantic Ocean caused significant amplification of the solar-induced atmospheric variations and thus resulted in climate changes in the low-latitudes (Bond et al., 2001; Wang et al., 2016). The studied site is located at the boundary of the Asian monsoons, which is an important link to the climate changes between the high- and low-latitudes of the Northern Hemisphere (Liu et al., 2020; Wang et al., 2017). The East Asian monsoons variability in this study was based on the stalagmite $\delta^{18}O$ (Dykoski et al., 2005).

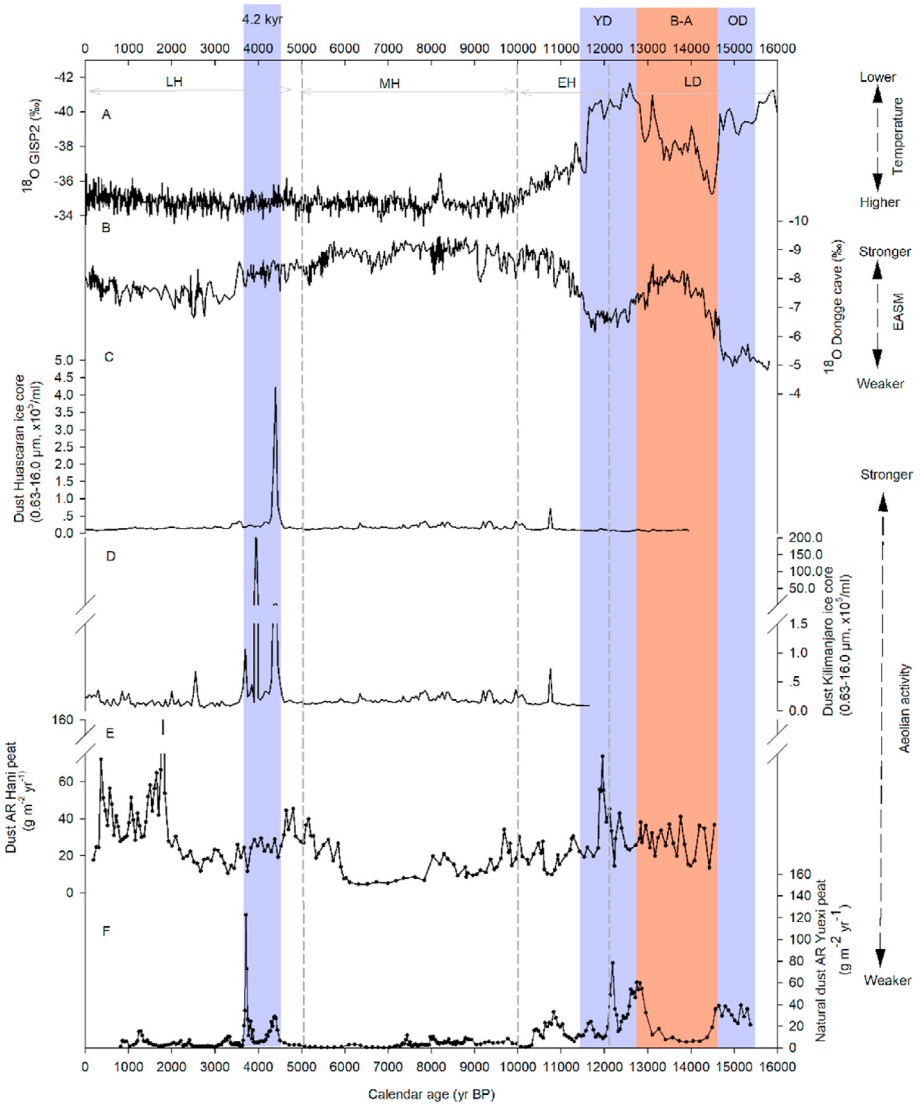

Fig. 8. Comparison of the dust record from Yuexi peat with other climatic proxies since the last deglaciation. 4.2 kyr, YD, B-A and OD represent 4.2 kyr cold event, Younger Dryas cold period, Bølling-Allerød warm periods, and Oldest Dryas, respectively. A: $\delta^{18}O$ record from the GISP2 ice core (Stuiver et al., 1995), B: stalagmite $\delta^{18}O$ from the Dongge Cave in south China (Dykoski et al., 2005), C: Ice core dust record from Huascarán in the Andes of Northern Peru (Thompson et al., 2000), D: Ice core dust record from Kilimanjaro in tropical Africa (Thompson et al., 2002), E: dust record from the Hani peat in northeast China (Pratte et al., 2020).

The Hani peat dust flux had been reported as an interplay proxy of the East Asian monsoons and the Westerlies (Pratte et al., 2020). These monsoon proxies correspond well to the natural dust record in the Yuexi peat (Fig. 8). Taking the provenance into account, the dust record in the Yuexi peat probably represents the climatic modulation of the East Asia monsoons.

In addition to these climatic mechanisms, the potential anthropogenic impacts should be considered, especially during the late Holocene because China has a long civilization history which was accompanied by periodical dynastic shifts. A recent study on lake sediment from Gonghai showed that dynastic changes dominated dust storm activity in eastern China in the past 2000 years (Chen et al., 2020a). In the Yuexi peatland, the dust flux increased during the unified and developed dynasties (Han, Tang and Song), and decreased during the war periods (early Qin, the Era of Disunity (220–589 C.E.), and the Five Dynasties and Ten Kingdoms period (5D & 10K, 907–979 C.E.). These generally agreed with the Gonghai record (Fig. 9). Besides, the variations in the concentrations of trace metals (Cu and Pb) were used to indicate past metal pollution from various human activities. Two peaks in the enrichment factors relative to the Upper Continental Crust were observed during Tang and Song dynasties, which were the most developed civilizations in ancient China. These proxies of anthropogenic impacts were consistent with the dust records both in the Yuexi peat and the Gonghai lake sediment (Chen et al., 2020a). Therefore, our results provide evidence of the human influence on the dust evolution in China during the late Holocene.

5. Conclusions

A high-resolution 8800-year atmospheric dust deposition history was reconstructed using major and trace elements records from the Yuexi ombrotrophic peatland. Provenance tracers Y/ΣREE, La/Yb, Y/Yb, Y/Er were in line with the deserts in northwest China, the Loess Plateau and the soils from the Tibetan Plateau, but showed no correlations with records from the Indian Thar desert, suggesting that long-distance dust transportation from northwest China was the dominant source of Yuexi peatland. The mineral dust

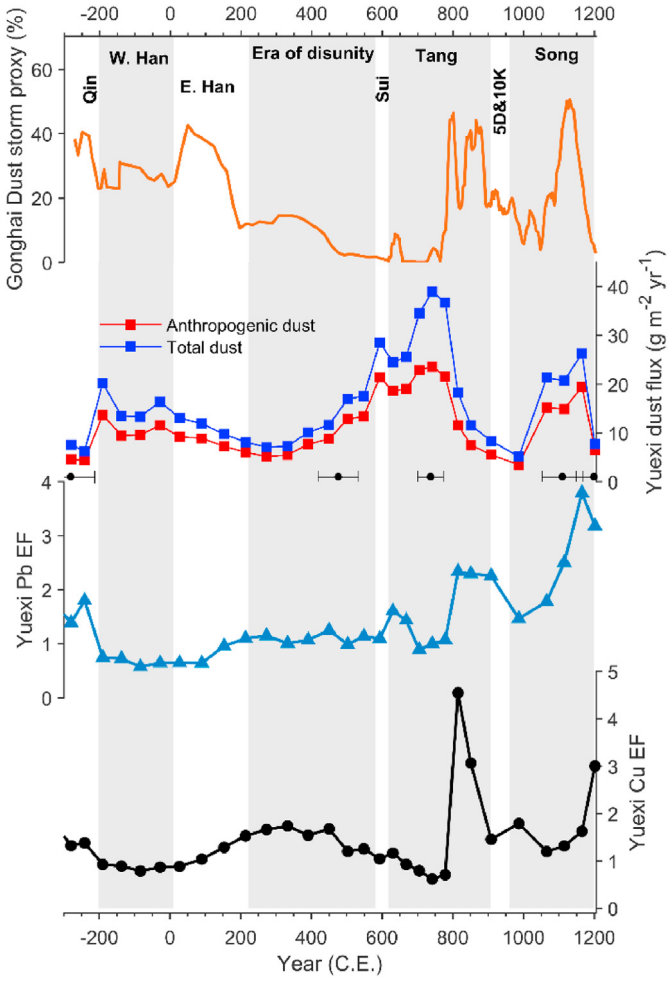

Fig. 9. Variations in the anthropogenic dust flux in the Yuexi peat and dust flux in Gonghai lake (Chen et al., 2020a) and the Yuexi peat over the last 2000 years. The temporal variations of Cu and Pb enrichment factors in the Yuexi peat were also included to indicate the anthropogenic impacts. The main Chinese dynasties are indicated by alternating grey and white columns and the raw radiocarbon age-control points with error bar are indicated below the dust flux.

flux was quite stable and low during the middle Holocene. Mean natural dust fluxes during the time interval 8800-5000 years BP was 3.8 g m^{-2} yr^{-1}, which could be an alternative baseline of long-term atmospheric dust flux in China. The Yuexi peat dust flux record displayed pronounced increases during the OD and YD intervals and the 4.2 kyr cold event period, which is in good agreement with global climatic records, suggesting that cooling events in the high latitudes are teleconnected with climate changes in southwest China. Our analysis shows that dust fluxes were correlated with the dynamics of Asian monsoon and North Atlantic climate, implying that climatic variabilities played an important role in modulating peatland long-term dust deposition. Besides, we also find that anthropogenic dust contributed significantly to the abrupt increases in the dust deposition rate during the Tang dynasty and the Song dynasty.

Author contributions

H.P., K.B., and B.H. designed the study and performed most of the analyses with support from L.Y., M.U., C.C., Y. Z., Q.G., H.D., H.Y., and Y.H. C.C., B.H., and Y.Z. conducted the sample collection. M.U., L.Y., Q.G., and H.D. contributed to laboratory analysis. H.P. and K.B. wrote the paper with input from B.H. All authors contributed to interpreting the results and discussions.

Declaration of competing interest

The authors declare that they have no known competing financial interests or personal relationships that could have appeared to influence the work reported in this paper.

Acknowledgements

We thank Nathalie Fagel and another anonymous reviewer for valuable comments and suggestions. This research was supported by the Strategic Priority Research Program of the Chinese Academy of Sciences (Grant No. XDB40000000) and the National Nature Science Foundation of China (Grants Nos. 41971113, 41907288, and 41673119). H.P. was supported by the CAS "Light of West China" Program and the CAS Scholarship.

References

Allan, M., Le Roux, G., Piotrowska, N., Beghin, J., Javaux, E., Court-Picon, M., Mattielli, N., Verheyden, S., Fagel, N., 2013. Mid- and late Holocene dust deposition in western Europe: the Misten peat bog (Hautes Fagnes - Belgium). Clim. Past 9, 2285–2298.

An, Z.S., Colman, S.M., Zhou, W.J., Li, X.Q., Brown, E.T., Jull, A.J.T., Cai, Y.J., Huang, Y.S., Lu, X.F., Chang, H., Song, Y.G., Sun, Y.B., Xu, H., Liu, W.G., Jin, Z.D., Liu, X.D., Cheng, P., Liu, Y., Ai, L., Li, X.Z., Liu, X.J., Yan, L.B., Shi, Z.G., Wang, X.L., Wu, F., Qiang, X.K., Dong, J.B., Lu, F.Y., Xu, X.W., 2012. Interplay between the westerlies and asian monsoon recorded in lake Qinghai sediments since 32 ka. Sci. Rep. 2.

Bao, K., Xia, W., Lu, X., Wang, G., 2010. Recent atmospheric lead deposition recorded in an ombrotrophic peat bog of Great Hinggan Mountains, Northeast China, from Pb-210 and Cs-137 dating. J. Environ. Radioact. 101, 773–779.

Bao, K.S., Xing, W., Yu, X.F., Zhao, H.M., McLaughlin, N., Lu, X.G., Wang, G.P., 2012. Recent atmospheric dust deposition in an ombrotrophic peat bog in Great Hinggan Mountain, Northeast China. Sci. Total Environ. 431, 33–45.

Blaauw, M., Christen, J.A., 2011. Flexible paleoclimate age-depth models using an autoregressive gamma process. Bayesian Analysis 6, 457–474.

Bond, G., Kromer, B., Beer, J., Muscheler, R., Evans, M.N., Showers, W., Hoffmann, S., Lotti-Bond, R., Hajdas, I., Bonani, G., 2001. Persistent solar influence on north Atlantic climate during the Holocene. Science 294, 2130–2136.

Chen, F.H., Chen, S.Q., Zhang, X., Chen, J.H., Wang, X., Gowan, E.J., Qiang, M.R., Dong, G.H., Wang, Z.L., Li, Y.C., Xu, Q.H., Xu, Y.Y., Smol, J.P., Liu, J.B., 2020a. Asian dust-storm activity dominated by Chinese dynasty changes since 2000 BP. Nat. Commun. 11.

Chen, X.Y., Blockley, S.P.E., Xu, Y.G., Menzies, M.A., 2020b. Holocene tephrostratigraphic framework and monsoon evolution of East Asia: Key tephra beds for synchronising palaeoclimate records. Quat. Sci. Rev. 242.

Compo, G.P., Whitaker, J.S., Sardeshmukh, P.D., 2006. Feasibility of a 100-year reanalysis using only surface pressure data. Bull. Am. Meteorol. Soc. 87, 175–190.

Cortizas, A.M., Lopez-Costas, O., Orme, L., Mighall, T., Kylander, M.E., Bindler, R., Sala, A.G., 2020. Holocene atmospheric dust deposition in NW Spain. Holocene 30, 507–518.

Cullen, H.M., deMenocal, P.B., Hemming, S., Hemming, G., Brown, F.H., Guilderson, T., Sirocko, F., 2000. Climate change and the collapse of the Akkadian empire: evidence from the deep sea. Geology 28, 379–382.

De Vleeschouwer, F., Ferrat, M., McGowan, H., Vanneste, H., Weiss, D., 2014. Extracting paleodust information from peat geochemistry. PAGES Magazine: Past Global Changes Magazine 22, 88–89.

Dykoski, C.A., Edwards, R.L., Cheng, H., Yuan, D.X., Cai, Y.J., Zhang, M.L., Lin, Y.S., Qing, J.M., An, Z.S., Revenaugh, J., 2005. A high-resolution, absolute-dated Holocene and deglacial Asian monsoon record from Dongge Cave, China. Earth Planet Sci. Lett. 233, 71–86.

Fagel, N., Allan, M., Le Roux, G., Mattielli, N., Piotrowska, N., Sikorski, J., 2014. Deciphering human-climate interactions in an ombrotrophic peat record: REE, Nd and Pb isotope signatures of dust supplies over the last 2500 years (Misten bog, Belgium). Geochem. Cosmochim. Acta 135, 288–306.

Ferrat, M., Weiss, D.J., Dong, S.F., Large, D.J., Spiro, B., Sun, Y.B., Gallagher, K., 2012a. Lead atmospheric deposition rates and isotopic trends in Asian dust during the last 9.5 kyr recorded in an ombrotrophic peat bog on the eastern Qinghai-Tibetan Plateau. Geochem. Cosmochim. Acta 82, 4–22.

Ferrat, M., Weiss, D.J., Spiro, B., Large, D., 2012b. The inorganic geochemistry of a peat deposit on the eastern Qinghai-Tibetan Plateau and insights into changing atmospheric circulation in central Asia during the Holocene. Geochem. Cosmochim. Acta 91, 7–31.

Ferrat, M., Weiss, D.J., Strekopytov, S., Dong, S.F., Chen, H.Y., Najorka, J., Sun, Y.B., Gupta, S., Tada, R., Sinha, R., 2011. Improved provenance tracing of Asian dust

sources using rare earth elements and selected trace elements for palaeomonsoon studies on the eastern Tibetan Plateau. Geochem. Cosmochim. Acta 75, 6374–6399.
Gao, Y., Xiong, K., Quan, M., Song, B., Peng, H., Peng, H., Shen, W., Bao, K., 2019. Holocene climate dynamics derived from pollen record of Jiulongchi wetland in Fanjing Mountain, southwest China. Quat. Int. 513, 1–7.
Hong, B., Gasse, F., Uchida, M., Hong, Y.T., Leng, X.T., Shibata, Y., An, N., Zhu, Y.X., Wang, Y., 2014a. Increasing summer rainfall in arid eastern-Central Asia over the past 8500 years. Sci. Rep. 4.
Hong, B., Hong, Y.T., Uchida, M., Shibata, Y.Y., Cai, C., Peng, H.J., Zhu, Y.X., Wang, Y., Yuan, L.G., 2014b. Abrupt variations of Indian and East Asian summer monsoons during the last deglacial stadial and interstadial. Quat. Sci. Rev. 97, 58–70.
Hong, B., Liu, C.Q., Lin, Q.H., Yasuyuki, S., Leng, X.T., Wang, Y., Zhu, Y.X., Hong, Y.T., 2009. Temperature evolution from the $\delta^{18}O$ record of Hani peat, Northeast China, in the last 14,000 years. Sci. China Earth Sci. 52, 952–964.
Hong, B., Uchida, M., Hong, Y.T., Peng, H.J., Kondo, M., Ding, H.W., 2018. The respective characteristics of millennial-scale changes of the India summer monsoon in the Holocene and the Last Glacial. Palaeogeogr. Palaeoclimatol. Palaeoecol. 496, 155–165.
Hong, Y.T., Hong, B., Lin, Q.H., Shibata, Y., Hirota, M., Zhu, Y.X., Leng, X.T., Wang, Y., Wang, H., Yi, L., 2005. Inverse phase oscillations between the East Asian and Indian Ocean summer monsoons during the last 12,000 years and paleo-El Niño. Earth Planet Sci. Lett. 231, 337–346.
Jiang, W.Y., Leroy, S.A.G., Yang, S.L., Zhang, E.L., Wang, L., Yang, X.X., Rioual, P., 2019. Synchronous strengthening of the Indian and East Asian monsoons in response to global warming since the last deglaciation. Geophys. Res. Lett. 46, 3944–3952.
Kohfeld, K.E., Harrison, S.P., 2001. DIRTMAP: the geological record of dust. Earth Sci. Rev. 54, 81–114.
Kylander, M.E., Bindler, R., Cortizas, A.M., Gallagher, K., Morth, C.M., Rauch, S., 2013. A novel geochemical approach to paleorecords of dust deposition and effective humidity: 8500 years of peat accumulation at Store Mosse (the "Great Bog"), Sweden. Quat. Sci. Rev. 69, 69–82.
Kylander, M.E., Martinez-Cortizas, A., Bindler, R., Greenwood, S.L., Morth, C.M., Rauch, S., 2016. Potentials and problems of building detailed dust records using peat archives: an example from Store Mosse (the "Great Bog"), Sweden. Geochem. Cosmochim. Acta 190, 156–174.
Kyotani, T., Koshimizu, S., Kobayashi, H., 2005. Short-term cycle of eolian dust (Kosa) recorded in Lake Kawaguchi sediments, central Japan. Atmos. Environ. 39, 3335–3342.
Le Roux, G., Fagel, N., De Vleeschouwer, F., Krachler, M., Debaille, V., Stille, P., Mattielli, N., van der Knaap, W.O., van Leeuwen, J.F.N., Shotyk, W., 2012. Volcano- and climate-driven changes in atmospheric dust sources and fluxes since the Late Glacial in Central Europe. Geology 40, 335–338.
Li, C.X., Sonke, J.E., Le Roux, G., Van der Putten, N., Piotrowska, N., Jeandel, C., Mattielli, N., Benoit, M., Wiggs, G.F.S., De Vleeschouwer, F., 2020. Holocene dynamics of the southern westerly winds over the Indian Ocean inferred from a peat dust deposition record. Quat. Sci. Rev. 231.
Li, Q., Liu, X., Wang, Z., Zheng, Y., 2016a. Distributions and environmental significance of GDGTs in modern peat samples from eastern Tibetan Plateau. Quat. Sci. 36, 388–395 (in Chinese with English abstract).
Li, Y.C., Zhang, M., Shu, M., Ho, S.S.H., Liu, Z.F., Wang, X.X., Zhao, X.Q., 2016b. Chemical characteristics of rainwater in Sichuan basin, a case study of Ya'an. Environ. Sci. Pollut. Control Ser. 23, 13088–13099.
Liu, X.X., Sun, Y.B., Vandenberghe, J., Cheng, P., Zhang, X., Gowan, E.J., Lohmann, G., An, Z.S., 2020. Centennial- to millennial-scale monsoon changes since the last deglaciation linked to solar activities and North Atlantic cooling. Clim. Past 16, 315–324.
Masson, O., Piga, D., Gurriaran, R., D'Amico, D., 2010. Impact of an exceptional Saharan dust outbreak in France: PM10 and artificial radionuclides concentrations in air and in dust deposit. Atmos. Environ. 44, 2478–2486.
McLennan, S.M., 1985. The Continental Crust: its Composition and Evolution: an Examination of the Geochemical Record Preserved in Sedimentary Rocks. Blackwell Scientific.
Pratte, S., Bao, K.S., Sapkota, A., Zhang, W.F., Shen, J., Le Roux, G., De Vleeschouwer, F., 2020. 14 kyr of atmospheric mineral dust deposition in northeastern China: a record of palaeoclimatic and palaeoenvironmental changes in the Chinese dust source regions. Holocene 30, 492–506.
Pratte, S., Garneau, M., De Vleeschouwer, F., 2017. Late-Holocene atmospheric dust deposition in eastern Canada (St. Lawrence North Shore). Holocene 27, 12–25.
Renssen, H., Seppa, H., Heiri, O., Roche, D.M., Goosse, H., Fichefet, T., 2009. The spatial and temporal complexity of the Holocene thermal maximum. Nat. Geosci. 2, 410–413.
Rhodes, T.E., Gasse, F., Lin, R.F., Fontes, J.C., Wei, K.Q., Bertrand, P., Gibert, E., Melieres, F., Tucholka, P., Wang, Z.X., Cheng, Z.Y., 1996. A late Pleistocene-Holocene lacustrine record from Lake Manas, Zunggar (northern Xinjiang, western China). Palaeogeogr. Palaeoclimatol. Palaeoecol. 120, 105–121.
Sapkota, A., Cheburkin, A.K., Bonani, G., Shotyk, W., 2007. Six millennia of atmospheric dust deposition in southern South America (Isla Navarino, Chile). Holocene 17, 561–572.
Shao, Y.P., Wyrwoll, K.H., Chappell, A., Huang, J.P., Lin, Z.H., McTainsh, G.H., Mikami, M., Tanaka, T.Y., Wang, X.L., Yoon, S., 2011. Dust cycle: an emerging core theme in Earth system science. Aeolian Research 2, 181–204.
Shi, Y.F., Shen, Y.P., Kang, E., Li, D.L., Ding, Y.J., Zhang, G.W., Hu, R.J., 2007. Recent and future climate change in northwest China. Climatic Change 80, 379–393.
Shotyk, W., 1996. Peat bog archives of atmospheric metal deposition: geochemical evaluation of peat profiles, natural variations in metal concentrations, and metal enrichment factors. Environ. Rev. 4, 149–183.
Shotyk, W., Krachler, M., Martinez-Cortizas, A., Cheburkin, A.K., Emons, H., 2002. A peat bog record of natural, pre-anthropogenic enrichments of trace elements in atmospheric aerosols since 12 370 14C yr BP, and their variation with Holocene climate change. Earth Planet Sci. Lett. 199, 21–37.
Shotyk, W., Weiss, D., Appleby, P.G., Cheburkin, A.K., Frei, R., Gloor, M., Kramers, J.D., Reese, S., Van der Knaap, W.O., 1998. History of atmospheric lead deposition since 12,370 ^{14}C yr BP from a peat bog, Jura Mountains, Switzerland. Science 281, 1635–1640.
SPSS, 2002. Statistical Product and Service Solution. SPSS Inc Chicago, IL, USA, version 11.5.
Steinmann, P., Shotyk, W., 1997. Geochemistry, mineralogy, and geochemical mass balance on major elements in two peat bog profiles (Jura Mountains: Switzerland). Chem. Geol. 138, 25–53.
Stuiver, M., Grootes, P.M., Braziunas, T.F., 1995. The GISP2 $\delta^{18}O$ climate record of the past 16,500 years and the role of the sun, ocean, and volcanoes. Quat. Res. 44, 341–354.
Thompson, L.G., Mosley-Thompson, E., Davis, M.E., Henderson, K.A., Brecher, H.H., Zagorodnov, V.S., Mashiotta, T.A., Lin, P.N., Mikhalenko, V.N., Hardy, D.R., Beer, J., 2002. Kilimanjaro ice core records: evidence of Holocene climate change in tropical Africa. Science 298, 589–593.
Thompson, L.G., Mosley-Thompson, E., Henderson, K.A., 2000. Ice-core palaeoclimate records in tropical south America since the last glacial maximum. J. Quat. Sci. 15, 377–394.
Vanneste, H., De Vleeschouwer, F., Bertrand, S., Martinez-Cortizas, A., Vanderstraeten, A., Mattielli, N., Coronato, A., Piotrowska, N., Jeandel, C., Le Roux, G., 2016. Elevated dust deposition in Tierra del Fuego (Chile) resulting from Neoglacial Darwin Cordillera glacier fluctuations. J. Quat. Sci. 31, 713–722.
Vinoj, V., Rasch, P.J., Wang, H., Yoon, J.-H., Ma, P.-L., Landu, K., Singh, B., 2014. Short-term modulation of Indian summer monsoon rainfall by West Asian dust. Nat. Geosci. 7, 308–313.
Wang, P.X., Wang, B., Cheng, H., Fasullo, J., Guo, Z.T., Kiefer, T., Liu, Z.Y., 2017. The global monsoon across time scales: mechanisms and outstanding issues. Earth Sci. Rev. 174, 84–121.
Wang, X.S., Chu, G.Q., Sheng, M., Zhang, S.Q., Li, J.H., Chen, Y., Tang, L., Su, Y.L., Pei, J.L., Yang, Z.Y., 2016. Millennial-scale Asian summer monsoon variations in South China since the last deglaciation. Earth Planet Sci. Lett. 451, 22–30.
Wedepohl, K.H., 1995. The composition of the continental crust. Geochem. Cosmochim. Acta 59, 1217–1232.
Xie, S.C., Evershed, R.P., Huang, X.Y., Zhu, Z.M., Pancost, R.D., Meyers, P.A., Gong, L.F., Hu, C.Y., Huang, J.H., Zhang, S.H., Gu, Y.S., Zhu, J.Y., 2013. Concordant monsoon-driven postglacial hydrological changes in peat and stalagmite records and their impacts on prehistoric cultures in central China. Geology 41, 827–830.
Yang, X.P., Scuderi, L., Paillou, P., Liu, Z.T., Li, H.W., Ren, X.Z., 2011. Quaternary environmental changes in the drylands of China - a critical review. Quat. Sci. Rev. 30, 3219–3233.
Zhang, J., Xu, H., Lan, J., Ai, L., Sheng, E., Yan, D., Zhou, K.e., Yu, K., Song, Y., Zhang, S., Torfstein, A., 2020a. Weakening dust storm intensity in arid central Asia due to global warming over the past 160 years. Front. Earth Sci. 8, 284.
Zhang, X.-X., Claiborn, C., Lei, J.-Q., Vaughan, J., Wu, S.-X., Li, S.-Y., Liu, L.-Y., Wang, Z.-F., Wang, Y.-D., Huang, S.-Y., Zhou, J., 2020b. Aeolian dust in Central Asia: spatial distribution and temporal variability. Atmos. Environ. 238, 117734.